Elastic Scattering of 96-Mev Protons*

G. GERSTEIN, J. NIEDERER, AND K. STRAUCH
Cyclotron Laboratory, Harvard University, Cambridge, Massachusetts
(Received July 10, 1957)

The elastic scattering of 96-Mev protons from C, Al, Cu, Ag, Ta, Pb, and Th has been investigated at laboratory angles between 3° and 60°. A range telescope with an over-all energy resolution of 2.8 Mev was used to obtain the energy distribution of scattered protons at each angle of observation. The energy distributions are analyzed to obtain values for (1) an "upper limit" to the elastic cross section which includes slightly inelastic events, and (2) an "extrapolated" elastic cross section in which inelastic events are subtracted by an extrapolation procedure. All targets show diffraction minima and Coulomb-nuclear interference effects. The depth of the diffraction minima in general increases with atomic number, except that Ta and Th have less pronounced minima than either Ag or Pb.

I. INTRODUCTION

IT is customary to use the optical model[1] to describe the elastic scattering of high-energy nucleons by nuclei. In this model, the scattering center is represented by a complex potential whose form, shape, size, and strength are determined from experimental results. An analysis of total and absorption neutron cross sections[2] yields values for the strength of the scattering potential, but these values are not unique because they depend on the potential size and shape which are only roughly determined by the integrated cross sections. Differential cross-section measurements out to large angles are required for a more precise determination of the size and shape of the scattering potential. The results of scattering measurements carried out with 96-Mev unpolarized protons and a variety of target elements are reported in this paper.

The choice of protons as the bombarding particles was the result of the desire to cover large scattering angles. At such angles the elastic and inelastic scattering cross sections are of comparable magnitude and a careful separation must be made.[3] Such an analysis requires an incident beam with a narrow energy width and a detector with good energy selectivity and high efficiency. These conditions are difficult to fulfill with neutrons, but can be obtained with protons. Although the energy resolution of the work reported here was not sufficient to unambiguously separate elastically scattered protons, reliable "upper limits" to the elastic scattering have been obtained and "extrapolated" elastic scattering cross sections could be calculated.

No direct information on the spin-orbit term present in the optical potential[4] can be obtained from experiments carried out with unpolarized protons. However, when the measurements reported here were carried out, no polarized beam with sufficient energy-resolution and intensity was available to carry out the desired measurements.

* Supported by the joint program of the Office of Naval Research and the U. S. Atomic Energy Commission.
[1] Fernbach, Serber, and Taylor, Phys. Rev. **75**, 1369 (1949).
[2] T. B. Taylor, Phys. Rev. **92**, 831 (1953).
[3] K. Strauch and F. Titus, Phys. Rev. **103**, 100 (1956).
[4] E. Fermi, Nuovo cimento **11**, 497 (1954).

II. APPARATUS AND METHOD

A. Experimental Arrangement and Apparatus

The experimental arrangement is shown in Fig. 1. The external cyclotron beam was collimated so that it was 1 inch high and $\frac{1}{2}$ inch wide at the scattering target with a maximum intensity of 10^7 protons per second and an energy width of 2.0 Mev. The target, larger than the incident beam, was located at the center of an evacuated cylindrical scattering chamber. The detector telescope could be accurately positioned at various angles with respect to the incident beam, and its distance from the target could be varied to change the angular resolution. The beam was monitored by a Faraday cup located behind the scattering equipment, and it was possible to insert an ionization chamber between the defining slit and the target for certain calibration runs (Sec. IIB).

The detection telescope consisted of ten scintillation counters and was similar to one described previously.[3] The defining scintillator was 1 inch$\times\frac{1}{2}$ inch and the polyethylene absorbers were placed behind the defining scintillator to improve the angular resolution. The electronic system and method of data recording have been already described.[3,5] By varying the amount of absorbers in the telescope, a range spectrum of scattered

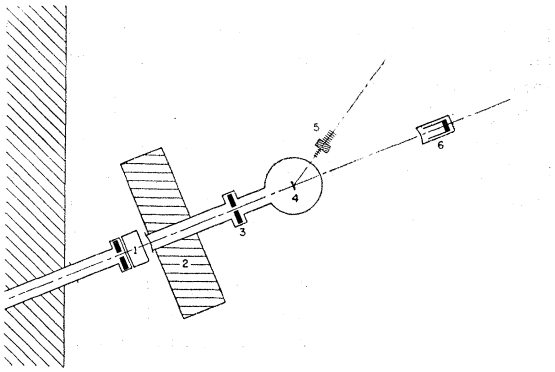

FIG. 1. Experimental arrangement. (1) Ionization chamber; (2) lead shield; (3) defining slit; (4) scattering chamber and target; (5) telescope; (6) Faraday cup.

[5] K. Strauch, Rev. Sci. Instr. **24**, 283 (1953).

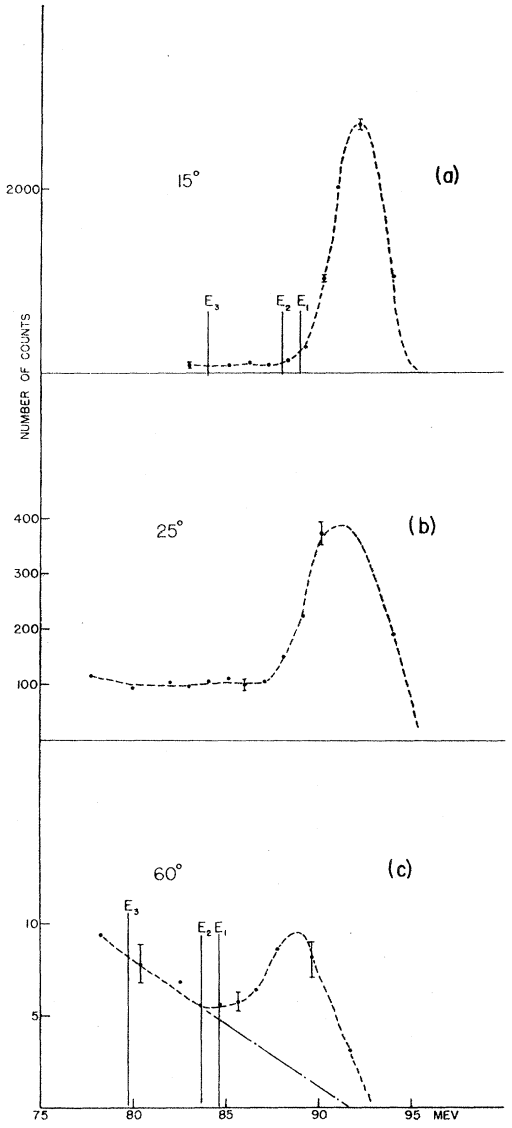

FIG. 2. Energy spectra from Al at various angles.

protons was obtained which was then converted into an energy spectrum.[3] Five range points were simultaneously obtained.

Targets had natural isotopic constitution and were made of standard laboratory purity materials. The thicknesses varied for different angular regions and were the result of a compromise between the desires for reasonable counting rates and minimum multiple scattering.

Combining the 2.1-Mev energy resolution of the telescope with the 2.0-Mev width of the incident beam gives an over-all energy resolution of 2.9 Mev.

B. Experimental Procedures

In each run the following steps were taken:

(1) The center of the scattering chamber was photographically aligned on the proton beam. A high-Z target was then inserted and the 0° telescope position determined by counting protons on both sides of the beam in a region of very rapidly varying differential cross section. This method is estimated to determine the 0° position to 5′.

(2) The efficiency of each counter was checked by the methods described previously.[3] The performance of the whole apparatus was checked by measuring $d\sigma/d\Omega$ for elastic scattering from carbon at 10°.

(3) A detailed range spectrum of protons scattered from the target under investigation was obtained at a fixed angle where there was little inelastic scattering. Two absorber sets were chosen so that the elastic peak started at the front and at the center of the telescope respectively.

(4) The telescope was set to various scattering angles in a well dispersed order to show up any slow drifts in the experimental conditions. At each angle data were taken with both sets of absorbers, yielding ten range points. Background readings were taken where necessary by rotating the target out of the beam.

(5) Step 2 was repeated.

With a target in place, multiple scattering spread the beam out of the solid angle which the Faraday cup could accept. To subtract background and to calculate an absolute cross section it was necessary to measure the fraction of the beam scattered out of the Faraday cup. This fraction was obtained from the change in ratio of charge accumulated by the Faraday cup to that by the ionization chamber under target-in and target-out conditions.

Special care was taken to compare the diffraction scattering from Ta and Pb, and from Pb and Th. In

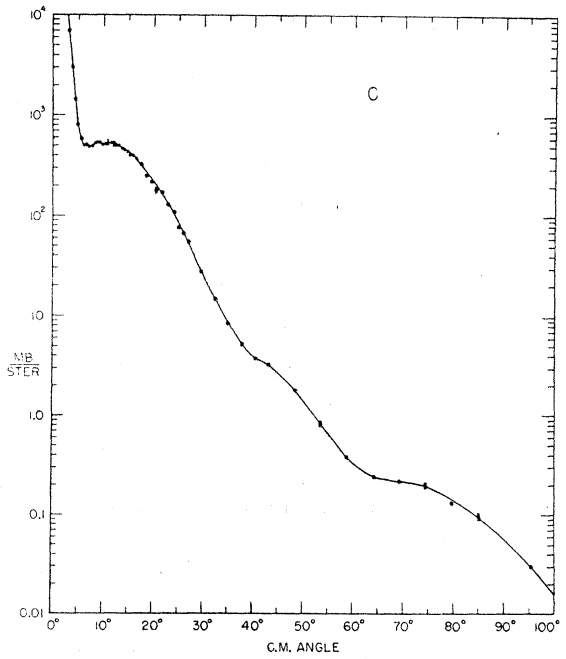

FIG. 3. Carbon elastic scattering differential cross section.

these cases readings were alternated between the two targets at each angle so that small differences would not be caused by changes in experimental conditions.

C. Estimates of Elastic Scattering

Three typical energy spectra obtained at well separated scattering angles are shown in Fig. 2. The points of the spectra taken at the larger angles have somewhat greater statistical errors because the data were obtained at a much lower counting rate. The energy resolution of the experiment was not sufficiently good to permit clear separation of elastic and low-lying inelastic events. (This remark does not apply to the carbon results that have been described previously.[3]) The results are therefore presented in two forms: (1) an "upper limit" to the elastic scattering cross section is calculated for each angle. (2) The inelastic contribution is estimated by extrapolation, and subtracted from the upper limit to yield an "extrapolated" elastic cross section.

At each angle of observation, a spectrum is obtained as explained in the preceding section and in Fig. 2. The elastic scattering cross section is proportional to the area under the high-energy peak, and this area is known with better percentage accuracy than each of the individual points that determine the exact spectrum shape.

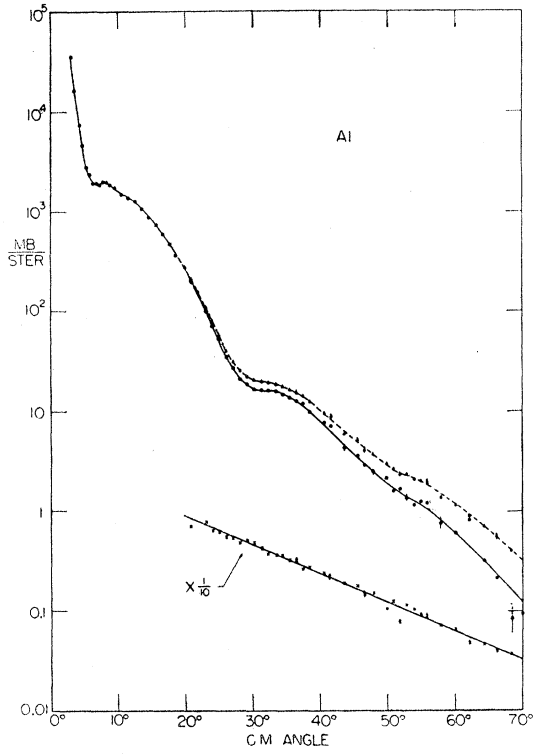

FIG. 4. Aluminum elastic scattering differential cross section. The dashed curve represents an "upper limit" to the elastic scattering cross section. The middle curve represents the "extrapolated" elastic scattering cross section. The lower curve represents the cross section for protons scattered inelastically into an approximately 4 Mev wide energy interval near the elastic peak.

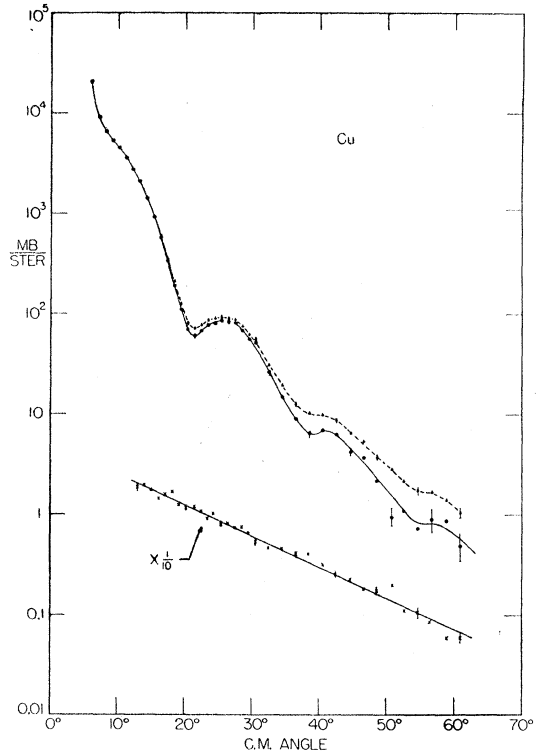

FIG. 5. Copper elastic scattering differential cross section. (See Fig. 4 caption.)

The beam intensity available made it impractical to measure accurately the shape of the energy spectrum at each of the larger scattering angles, and only the peak area was obtained to the desired accuracy. The following procedures were then used to extract the elastic scattering cross sections from the observations.

An accurately known small-angle spectrum was used to define E_1, the energy below which no elastically scattered protons appeared [Fig. 2(a)]. Taking nuclear recoil into account, the energy corresponding to E_1 was then calculated for each angle, and all protons with an energy larger than this were included in the calculation of the "upper limit" to the elastic differential cross section.

Unless the lowest lying levels of the target nuclei are excited very much more strongly than those lying 3 Mev or more above the ground state, this upper limit should correspond quite closely to the true elastic scattering cross section for small scattering angles. In the example of Fig. 2 inelastic events begin to contribute significantly to the area under the elastic peak at angles above 20°. This contribution is estimated by assuming that the number of inelastic events included in the elastic peak decreases with increasing energy at the same rate as corresponding events below E_1. The following procedure is used to obtain this estimate:

(1) Two convenient energy values E_2 and E_3 are chosen to include an approximately 4-Mev wide in-

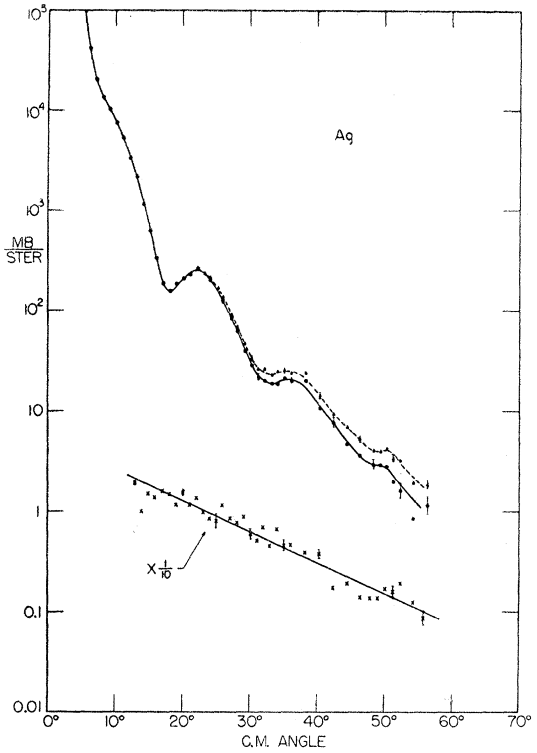

FIG. 6. Silver elastic scattering differential cross section. (See Fig. 4 caption.)

elastic region close to the elastic peak [Fig. 2(a)]. The lower curves of Figs. 3–9 show the angular distribution of these inelastically scattered protons.

(2) For each element, eight spectra covering angles larger than 20° are used to extrapolate the inelastic continuum from E_1 to the maximum energy that an inelastically scattered proton can have [Fig. 2(C)].

(3) It is found that the ratio R of the extrapolated area above E_1 to the area between E_2 and E_3 is essentially constant for a given element. As a result we obtain the extrapolated elastic scattering cross section at each angle by subtracting $R\times$(area between E_2 and E_3) from the area under the elastic peak.

This procedure is valid only if the inelastic scattering cross section is a smoothly decreasing function of the scattered proton energy. This seems to be the case from our results for protons that lose 3 or more Mev. No information is available to check this assumption for inelastically scattered protons corresponding to states of very low energy in the target nucleus.

The correction is important only at the larger scattering angles. In the 50°–60° region the estimated inelastic area under the elastic peak is about half of the peak area. Details of the differential cross-section shape and the location of minima are, however, largely independent of the inelastic correction as can be seen on Figs. 3–9.

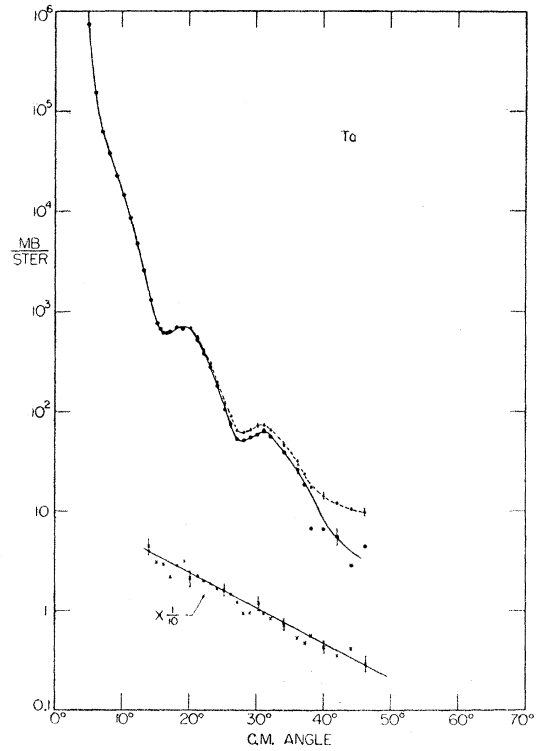

FIG. 7. Tantalum elastic scattering differential cross section. (See Fig. 4 caption.)

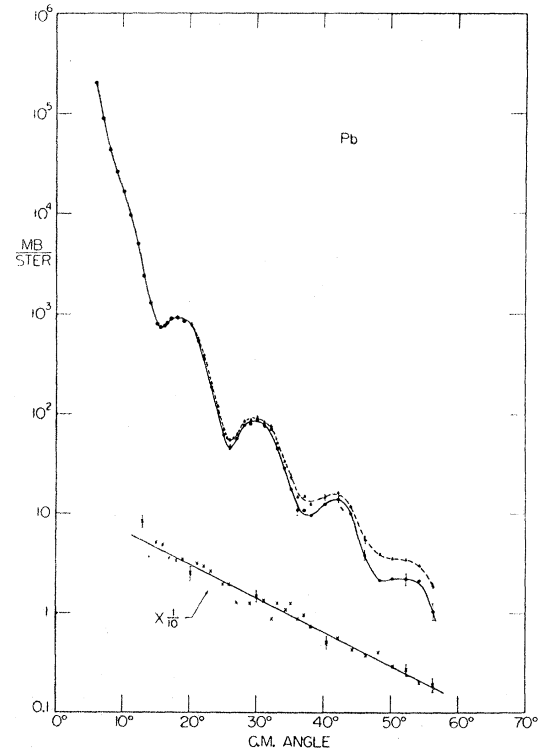

FIG. 8. Lead elastic scattering differential cross section. (See Fig. 4 caption.)

TABLE I. Incident energy (lab), target thickness, energy (c.m.) at target center, and angular resolution, for the angular ranges specified.

Element	Incident energy (lab) in Mev		Target thickness in Mev		Energy (c.m.) at target center, with uncertainty due to target thickness, in Mev		Angular resolution	
C	3°–14°	91.8		0.255	10.9°	84.5±0.12	3°–14°	0.7°
	14°–25°	92.2		3.73	21.7°	82.6±1.7	14°–25°	1.1°
	25°–100°	99.5		9.5	32.4°	87.5±4 5	25°–30°	1.9°
					64.2°	86.9±5.1	32.5°–100°	2.7°
					85.2°	86.2±5.8		
Al	3°–15°	92.9		0.397	10.4°	89.3±0.19	3°–15°	0.7°
	15°–20°	92.9		1.54	15.6°	88.6±0.74	15°–20°	1.1°
	20°–70°	95.7		6.57	26.0°	88.5±3.15	20°–70°	2.9°
Cu	all angles	95.6		2.31		93.0±1.11		3°
Ag	all angles	95.2		1.07		93.8±0.53		2.9°
Ta	all angles	94.8		0.695		93.9±0.35		2.8°
Pb	all angles	95.4	6°–44°	0.612		94.6±0.30		2.9°
			46°–56°	1.26		94.3±0.63		3.6°
Th	all angles	94.7		0.472		94.1±0.23		2.8°

D. Absolute Cross Sections and Angular Resolution

To calculate cross sections from the observed counting rates, corrections for outscattering and nuclear absorption in the telescope have to be applied. By moving the telescope into the direct beam these corrections were found to amount to 10–12%. The corrections were proportional to the amount of absorber and varied slightly within the telescope because of slight differences in outscattering.

Errors indicated on the elastic scattering cross section are purely statistical. On the middle curves representing the extrapolated elastic scattering cross section the statistical uncertainty due to the 4-Mev inelastic section is included. No estimate of the uncertainty in R has been made.

As explained in II B, the results for each element were obtained relative to the elastic scattering cross section for C at 10°. This cross section in turn has been compared to the proton-proton cross section at 40° (center-of-mass) measured with the same equipment using the CH_2-C method. This proton-proton cross section is known from the work of Kruse, Teem, and Ramsey,[6] and all our results are normalized to their value of 4.92±0.25% mb/sterad. The estimated internal consistency of our absolute cross sections is ±3%.

The angular resolution is primarily determined by three factors: the solid angle subtended by the defining scintillator, the size of the beam at the target, and the multiple scattering in the target. Some adjustments of these factors could be made, and they were chosen so as to maximize the counting rate for a given angular resolution. The angular resolution varied with targets and angles, and is indicated in Table I.

[6] Kruse, Teem, and Ramsey, Phys. Rev. **101**, 1079 (1956).

III. RESULTS AND DISCUSSION

The center-of-mass results for C, Al, Cu, Ag, Ta, Pb, and Th are shown in Figs. 3–9. The carbon results have been reported briefly in reference 3. In Figs. 4–9 the upper curve represents the "upper limit" to the elastic scattering cross section, the middle curve represents the extrapolated elastic scattering cross section, and the lower curve includes all protons scattered into the interval E_2-E_3. The Ta and Th results were not carried out to as high a scattering angle as other elements since

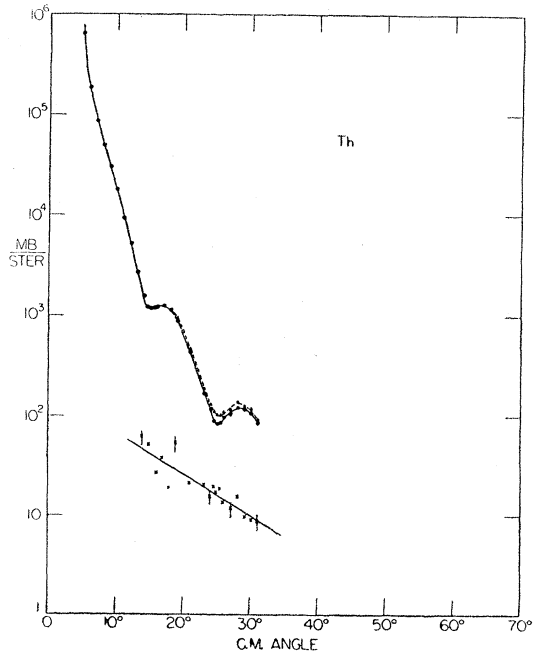

FIG. 9. Thorium elastic scattering differential cross section. (See Fig. 4 caption.)

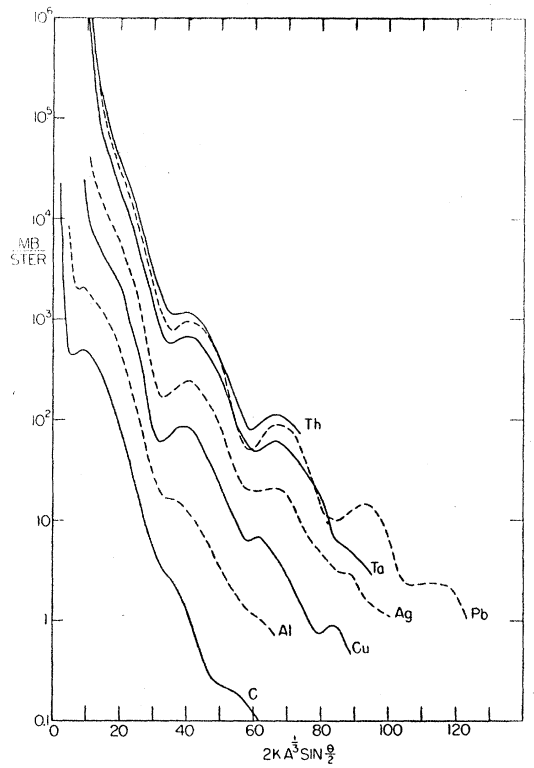

FIG. 10. Elastic scattering differential cross section as a function of $x=2kA^{\frac{1}{3}}\sin(\theta/2)$.

they were obtained primarily to compare the first and second diffraction minima with those of Pb.[7] Table I shows angular resolution and energy at the target center with the energy uncertainty caused by target thickness. These quantities varied because thicker targets were used for large-angle scattering.

Exact calculations are required to obtain the parameters of the optical model that best fit our data, since the WKB phase shifts are not sufficiently accurate. Such calculations are now being carried out by A. E. Glassgold and will be reported by him. However, it seems worthwhile to point out some features of the results presented here.

A region of destructive interference between nuclear and Coulomb scattering occurs at small angles and is especially marked in low-A elements. High-A elements show only a point of inflection.

The depth of the diffraction minima increases in general with increasing A. C shows only points of inflection, while deep minima and secondary maxima are seen in Pb. However, Ta ($A\approx 181$) and Th ($A\approx 232$) do not have as deep minima as Ag ($A\approx 108$) and Pb ($A\approx 207$). The depth of the first and second minima are not believed to be influenced very much by the experimental angular resolution. A measurement made with Pb using an angular resolution of about 1.5° shows the first minimum to be only slightly deeper than the 2.8° resolution results. These general features are similar to the high-energy electron elastic scattering results[8] of the Stanford group, and can be understood qualitatively by assuming that the smooth edge represents a smaller fraction of the projected nuclear area for high-A elements than for low-A elements. The Ta and Th anomalies are then due to the strong excitation of very low-lying rotational levels, or to the effect of the strong ellipsoidal deformation of these nuclei,[8] or to both. It is worth noting that the height of the secondary maxima in Ta and Th does not seem to be increased appreciably over that expected from a smooth A variation.

To point out the similarities and differences between the various spectra more clearly, they have all been plotted in Fig. 10 as a function of the parameter $x=2kA^{\frac{1}{3}}\sin(\theta/2)$, where all symbols have their usual meaning. Black-sphere scattering is a function of x only, but predicts much deeper minima than are observed. It is noted that the position of the observed diffraction minima and secondary maxima of the various elements depend on x to a good degree of approximation. The main exception to this statement is the position of the first minimum for the elements of highest A, which is probably influenced appreciably by Coulomb scattering.

We would like to thank Mr. P. Willmann for his help in the extensive data reduction. This work would not have been possible without the fine cooperation of the entire staff of the Cyclotron Laboratory.

[7] Tabulations of the results are available from this laboratory.

[8] R. Hofstadter, Revs. Modern Phys. **28**, 214 (1956).